Caustics, Critical Curves and Cross Sections for Gravitational Lensing by Disk Galaxies

Yun Wang and Edwin L. Turner

Princeton University Observatory

Peyton Hall, Princeton, NJ 08544

email: ywang,elt@astro.princeton.edu

arXiv:astro-ph/9702078v2 28 Aug 1997

Abstract

We study strong gravitational lensing by spiral galaxies, modeling them as infinitely thin uniform disks embedded in singular isothermal spheres. We derive general properties of the critical curves and caustics analytically. The multiple-image cross section is a sensitive function of the inclination angle of the disk relative to the observer. We compute the inclination averaged cross section for several sets of lensing parameters. For realistic disk mass and size parameters, we find that the cross section for multiple imaging is increased by only a modest factor and *no* dramatic increase in the optical depth for strong lensing of QSOs would be expected. However, the cross section for high magnifications is significantly increased due to the inclusion of a disk, especially for nearly edge-on configurations; due to the strong observational selection

effects favoring high magnifications, there might be significant consequences for lensing statistics.

1. Introduction

Early theoretical studies of gravitational lensing of distant quasars by foreground galaxies approximated their mass distributions as spherical and usually also as singular and isothermal (Gott & Gunn 1974; Turner 1980; Turner, Ostriker & Gott 1984). Later studies explored the relaxation of these simplifying approximations and, in particular, considered elliptical mass distributions and potentials (*e.g.*, Blandford & Kochanek 1987, Kochanek & Blandford 1987, Blandford & Narayan 1992), but it has been shown that the standard spherical approximations are adequate for the purpose of many statistical calculations (*e.g.*, Fukugita & Turner 1991, Maoz & Rix 1993, Kochanek 1993). However, with rare exception (Ostriker & Vietri 1990), the gravitational lensing effects of the defining component of spiral galaxies, their very thin disks, has been ignored in discussions of lensing statistics. There are two reasons. First, *within the limitations of the spherical galaxy approximation*, it was early shown (Turner et al. 1984) and later repeatedly confirmed by more detailed studies (Fukugita & Turner 1991, Kochanek 1991) that spiral galaxies contribute only a small fraction, of order 10%, of the total lensing cross section of the known galaxy population, with ellipticals and S0's being the dominant contributors. Second, the disk stability arguments originated by Ostriker & Peebles (1973) and the many other lines of evidence which indicate the presence of massive dark halos suggest that even spiral galaxy mass distributions are dominated by a roughly spherical component.

While these considerations remain valid, there now seem to be some reasons to examine

the lensing effects of thin disk mass distributions more carefully. For one, samples of galaxy lensed quasars are becoming rapidly larger and better controlled. Thus, smaller and more subtle features of lens statistics are becoming observationally accessible and therefore theoretically interesting. For another, in the usual (and very accurate) *thin lens* approximation, it is not the three dimensional mass distribution of the lensing object that matters but rather the projected two dimensional one, particularly those regions which exceed the lensing critical surface density (Turner et al. 1984). From this two dimensional point of view, a very thin disk may be much more important when seen nearly edge-on than it is in three dimensions. Finally, although the situation is far from unambiguous, observations suggest that lensing galaxies may have more dust (Lawrence et al. 1995, Malhotra, Rhoads & Turner 1997) and larger quadrupole mements (Keeton, Kochanek & Seljak 1996) than would have been naively expected if early type galaxies entirely dominated the quasar-galaxy lensing rate.

Therefore, in this paper we present a preliminary exploration of the lensing properties of spiral galaxies, which we approximate as finite, uniform surface density disks of zero thickness embedded in singular isothermal spheres (SIS). We focus on the general caustic and critical line properties of such lensing objects and also study the lensing cross section enhancement over the SIS only approximation. We explicitly carry the important variable of disk inclination angle throughout the calculations. In the present paper, however, we do not present the fully detailed calculations required for direct comparison to observations; in particular, we do not here consider line-of-sight integrations, integration over realistic

distributions of galaxy properties nor the effects of amplification (magnification) bias on observed samples. Rather, we present only an initial qualitative and semi-quantitative investigation of lensing by disk galaxy mass distributions.

The basic equations and model are presented in section 2. Section 3 discusses our technique for finding caustics, critical curves and multiple imaging configurations. Section 4 presents the general lensing properties of our model of disk galaxies in the language of caustics and critical curves. Section 5 considers the effects of inclined disks on lensing cross sections and the implied modification of quasar lensing rates. Finally, section 6 contains a summary of our results and a discussion of recent related work. We follow the conventions and notation of Schneider, Ehlers & Falco (1992).

2. Light deflection due to a spiral galaxy

We model spiral galaxies as uniform and infinitely thin disks embedded in singular isothermal spheres. Let us choose a length scale appropriate for a singular isothermal sphere (SIS),

$$\xi_0 = 4\pi \left(\frac{v_{SIS}}{c}\right)^2 \frac{D_d D_{ds}}{D_s}, \tag{1}$$

where v_{SIS} is the line-of-sight velocity dispersion of the SIS. Let $\boldsymbol{\xi}$ and $\boldsymbol{\eta}$ be the physical position vectors of the image (in the lens plane) and the source (in the source plane) respectively, then the dimensionless image and source positions are

$$\mathbf{x} = \frac{\boldsymbol{\xi}}{\xi_0}; \qquad \mathbf{y} = \frac{\boldsymbol{\eta}}{\eta_0}, \tag{2}$$

where $\eta_0 = \xi_0 D_s/D_d$, D_s and D_d are our distances to the source and lens respectively. The lens equation becomes

$$\mathbf{y} = \mathbf{x} - \boldsymbol{\alpha}(\mathbf{x}), \tag{3}$$

The scaled deflection angle

$$\boldsymbol{\alpha}(\mathbf{x}) = \frac{1}{\pi} \int \mathrm{d}^2 x' \, \kappa(\mathbf{x}') \frac{\mathbf{x} - \mathbf{x}'}{|\mathbf{x} - \mathbf{x}'|^2}, \tag{4}$$

where $\kappa(\mathbf{x}) = \Sigma(\xi_0 \mathbf{x})/\Sigma_{crit}$, with $\Sigma_{crit} = c^2 D_s/(4\pi G D_d D_{ds})$. D_{ds} is the distance between the lens and the source. We use affine distances, $D_d = cH_0^{-1}\lambda(z_d)$, $D_s = cH_0^{-1}\lambda(z_s)$, $D_{ds} = cH_0^{-1}\lambda(z_d, z_s) = cH_0^{-1}(1 + z_d)[\lambda(z_s) - \lambda(z_d)]$, where

$$\lambda(z) = \int_0^z \mathrm{d}w \, \frac{1}{(1+w)^2 \sqrt{\Omega_0(1+w)^3 + \Omega_\Lambda}}. \tag{5}$$

For $\Omega_0 = 1$, $\lambda(z) = (2/5)\left[1 - (1+z)^{-5/2}\right]$.

For a SIS, its dimensionless surface density and scaled deflection angle are (Schneider et al. 1992)

$$\kappa^{SIS}(\mathbf{x}) = \frac{1}{2|\mathbf{x}|}; \qquad \boldsymbol{\alpha}^{SIS}(\mathbf{x}) = \frac{\mathbf{x}}{|\mathbf{x}|}. \tag{6}$$

The projection of a circular disk of radius r_{disk} in the plane perpendicular to the line of sight is an ellipse with semi-major axes r_{disk} and $r_{disk} \cos\theta$, where θ is the angle between the normal vector of the inclined disk plane and the line of sight. Note that $0 \leq \theta \leq \pi/2$; $\theta = 0$ is the "face-on" disk case; $\theta = \pi/2$ is the "edge-on" disk case.

For a uniform disk, its projected surface density is $\Sigma_{disk} = M_{disk}/(\pi r_{disk}^2 \cos\theta)$; its

projected dimensionless surface density is

$$
\begin{aligned}
\kappa^{disk} &= \frac{\Sigma_{disk}}{\Sigma_{crit}} = \frac{1}{r_{disk}^2 \cos\theta} \frac{4GM_{disk}\, D_d D_{ds}}{c^2 D_s}, \\
&= \frac{0.19}{\cos\theta} \left(\frac{10\,\text{kpc}}{r_{disk}}\right)^2 \left(\frac{M_{disk}}{10^{11}\, M_\odot}\right) \left(\frac{D_d}{1000\,\text{Mpc}}\right) \frac{D_{ds}}{D_s}.
\end{aligned}
\tag{7}
$$

For simplicity in notation, we define

$$
q = \kappa^{disk} \cos\theta.
\tag{8}
$$

q is the *face-on* surface mass density of the disk. Note that $q < 1$ for realistic choices of the parameters.

The dimensionless radius of the disk is

$$
R = \frac{r_{disk}}{\xi_0} = \frac{10}{\pi} \left(\frac{r_{disk}}{10\,\text{kpc}}\right) \left(\frac{150\,\text{km/s}}{v_{SIS}}\right)^2 \left(\frac{1000\,\text{Mpc}}{D_d}\right) \frac{D_s}{D_{ds}}.
\tag{9}
$$

Let us choose the $\mathbf{x}$ coordinates such that the contour of the projected disk is given by

$$
\left(\frac{x_1}{R}\right)^2 + \left(\frac{x_2}{R\cos\theta}\right)^2 = 1.
\tag{10}
$$

Then the total scaled deflection angle $\boldsymbol{\alpha} = \boldsymbol{\alpha}^{SIS} + \boldsymbol{\alpha}^{disk}$, with $\boldsymbol{\alpha}^{disk}$ given by

$$
\begin{aligned}
\alpha_1^{disk} &= \frac{R\,q}{2\pi} \int_{-1}^{1} \mathrm{d}\omega\, \ln\left[\frac{(\sqrt{1-\omega^2}+x_1/R)^2 + (\omega\cos\theta - x_2/R)^2}{(\sqrt{1-\omega^2}-x_1/R)^2 + (\omega\cos\theta - x_2/R)^2}\right], \\
\alpha_2^{disk} &= \frac{R\,q}{2\pi\cos\theta} \int_{-1}^{1} \mathrm{d}\omega\, \ln\left[\frac{(\omega - x_1/R)^2 + (\sqrt{1-\omega^2}\cos\theta + x_2/R)^2}{(\omega - x_1/R)^2 + (\sqrt{1-\omega^2}\cos\theta - x_2/R)^2}\right].
\end{aligned}
\tag{11}
$$

Note that

$$
\alpha_2^{disk}(\cos\theta \to 0) = \frac{2x_2 q}{\pi} \int_{-1}^{1} \mathrm{d}\omega\, \frac{\sqrt{1-\omega^2}}{(\omega - x_1/R)^2 + (\sqrt{1-\omega^2}\cos\theta - x_2/R)^2}.
\tag{12}
$$

To study image multiplicity, we will also need the derivatives of the deflection angles:

$$
\begin{aligned}
\frac{\partial \alpha_1}{\partial x_1} &= \frac{2q}{\pi} \int_{-1}^{1} d\omega \, \frac{\sqrt{1-\omega^2}}{f_1(\omega)} \left[1 - \omega^2 - \left(\frac{x_1}{R}\right)^2 + \left(\frac{x_2}{R} - \omega \cos\theta\right)^2 \right] + \frac{x_2^2}{x^3}, \\
\frac{\partial \alpha_1}{\partial x_2} &= -\frac{4q}{\pi} \left(\frac{x_1}{R}\right) \int_{-1}^{1} d\omega \, \frac{\sqrt{1-\omega^2}}{f_1(\omega)} \left(\frac{x_2}{R} - \omega \cos\theta\right) - \frac{x_1 x_2}{x^3}, \\
\frac{\partial \alpha_2}{\partial x_1} &= -\frac{4q}{\pi} \left(\frac{x_2}{R}\right) \int_{-1}^{1} d\omega \, \frac{\sqrt{1-\omega^2}}{f_2(\omega)} \left(\frac{x_1}{R} - \omega\right) - \frac{x_1 x_2}{x^3}, \\
\frac{\partial \alpha_2}{\partial x_2} &= \frac{2q}{\pi} \int_{-1}^{1} d\omega \, \frac{\sqrt{1-\omega^2}}{f_2(\omega)} \left[\left(\frac{x_1}{R} - \omega\right)^2 - \left(\frac{x_2}{R}\right)^2 + (1-\omega^2)\cos^2\theta \right] + \frac{x_1^2}{x^3}.
\end{aligned}
\tag{13}
$$

We have defined

$$
\begin{aligned}
f_1(\omega) &\equiv \left[\left(\frac{x_1}{R} + \sqrt{1-\omega^2}\right)^2 + \left(\frac{x_2}{R} - \omega \cos\theta\right)^2 \right] \left[\left(\frac{x_1}{R} - \sqrt{1-\omega^2}\right)^2 + \left(\frac{x_2}{R} - \omega \cos\theta\right)^2 \right], \\
f_2(\omega) &\equiv \left[\left(\frac{x_1}{R} - \omega\right)^2 + \left(\frac{x_2}{R} + \sqrt{1-\omega^2}\cos\theta\right)^2 \right] \left[\left(\frac{x_1}{R} - \omega\right)^2 + \left(\frac{x_2}{R} - \sqrt{1-\omega^2}\cos\theta\right)^2 \right].
\end{aligned}
$$

$$\tag{14}$$

3. Condition for multiple images

The magnification factor of the source is given by $\mu(\mathbf{x}) = 1/\det A(\mathbf{x})$, where the Jacobian matrix $A(\mathbf{x})$ is defined as

$$
A(\mathbf{x}) = \frac{\partial \mathbf{y}}{\partial \mathbf{x}}, \qquad A_{ij} = \frac{\partial y_i}{\partial x_j};
\tag{15}
$$

$$
\det A = \left(1 - \frac{\partial \alpha_1}{\partial x_1}\right)\left(1 - \frac{\partial \alpha_2}{\partial x_2}\right) - \frac{\partial \alpha_1}{\partial x_2} \cdot \frac{\partial \alpha_2}{\partial x_1}.
$$

It has been shown that an isolated transparent lens can produce multiple images if, and only if, there is a point $\mathbf{x}$ with $\det A(\mathbf{x}) < 0$. If at $\mathbf{x}_0$, $\det A(\mathbf{x}_0) < 0$ (negative parity), a source at $\mathbf{y}_0 = \mathbf{y}(\mathbf{x}_0)$ has at least two additional images of positive parity. The

multiple-image cross-section is simply the bounded area in the source plane in which for each source position $\mathbf{y}$, there exists an image position $\mathbf{x}$ where $\det A(\mathbf{x}) < 0$.

Formally, critical curves are given by $\det A(\mathbf{x}) = 0$, the corresponding source positions are the caustics. However, the cross-section for multiple images is not always bounded by a caustic. In the case of SIS only, $\det A = 1 - 1/x$, where $x = \sqrt{x_1^2 + x_2^2}$. $\det A < 0$ gives $0 \leq x < 1$. The lens equation gives us $y = |x - 1|$. Hence $y \leq 1$ for multiple images; the multiple image cross-section is bounded by $y = 1$, which corresponds to $x = 0$ (where $\det A = -\infty$), while the only critical curve is at $x = 1$ corresponding to $y = 0$.

Next let us consider the case of SIS plus a face-on disk, $\theta = 0$, $\kappa^{disk} = q$. It's straightforward to integrate Eqs.(11) to find (Schneider et al. 1992)

$$\boldsymbol{\alpha} = \begin{cases} \mathbf{x}/x + \kappa^{disk}\,\mathbf{x}, & x < R; \\[2mm] \mathbf{x}/x + \kappa^{disk}R^2\,\mathbf{x}/x^2, & x > R. \end{cases} \tag{16}$$

Hence we have

$$\det A = \begin{cases} \left(1 - \kappa^{disk}\right)\left(1 - \kappa^{disk} - 1/x\right), & x < R; \\[2mm] \left(1 + \kappa^{disk}R^2/x^2\right)\left(1 - 1/x - \kappa^{disk}R^2/x^2\right), & x > R. \end{cases} \tag{17}$$

It is easy to see that $\det A$ is *discontinuous* at $x = R$.

For $\kappa^{disk} < 1$, $\det A$ does *not* change sign at $x = R$. If $R > 1/(1 - \kappa^{disk})$, the only critical curve is given by $x = 1/(1 - \kappa^{disk}) < R$, and it maps to $y = 0$; if $R < 1/(1 - \kappa^{disk})$, the only critical curve is given by $x = \left(1 + \sqrt{1 + 4\kappa^{disk}R^2}\right)/2 > R$, and it also maps to $y = 0$. The critical curves therefore have no relevance to image multiplicity. On the other

hand, $\det A(x) < 0$ leads to $y \leq 1$, with $y = 1$ given by $x = 0$, just as in the SIS only case. SIS with a face-on disk of $\kappa^{disk} < 1$ has the same multiple-image cross section as SIS only.

If $\kappa^{disk} > 1$, the true critical curve is given by $x = (1 + \sqrt{1 + 4\kappa^{disk}R^2})/2 > R$, which again maps to $y = 0$. However, $\det A(x < R) > 0$, $\det A(x \to R^+) < 0$, hence $\det A$ changes sign at $x = R$, which is effectively a "critical curve"; the corresponding "caustic" is given by $y = 1 + R(\kappa^{disk} - 1) > 1$. SIS with a face-on disk of $\kappa^{disk} > 1$ has a larger multiple-image cross section than SIS only.

4. Image multiplicity for SIS plus inclined disk

For SIS plus uniform disk, $\boldsymbol{\alpha}^{disk}(x = 0) = 0$, hence $x = 0$ corresponds to source position $y = 1$, just as in the SIS only case. When $\det A(x \to 0) < 0$, $y \leq 1$ always gives multiple images; the multiple-image cross-section increases relative to the SIS only case if any caustic curves lie outside the $y = 1$ circle.

The value of $\det A$ at $x = 0$ is a useful indicator of the general properties of the critical curves. For uniform disk plus SIS, we find [using Eqs.(13) and (15)]

$$\det A(x \to 0) = 1 - \frac{2q}{\cos\theta} + \frac{1}{\cos\theta}\left(\frac{2q}{1+\cos\theta}\right)^2 + \frac{C_1(\theta)\, x_1^2}{x^3} + \frac{C_2(\theta)\, x_2^2}{x^3}, \tag{18}$$

where

$$C_1(\theta) = \frac{2q}{1+\cos\theta} - 1, \qquad C_2(\theta) = \frac{2q}{\cos\theta(1+\cos\theta)} - 1. \tag{19}$$

Let us define

$$S \equiv C_1 x_1^2 + C_2 x_2^2. \tag{20}$$

S has the same sign as $\det A(x \to 0)$. We have two critical angles:

$$C_1(\theta) = 0: \qquad \theta = \theta_1 = \arccos(2q - 1);$$

$$C_2(\theta) = 0: \qquad \theta = \theta_2 = \arccos\left(\frac{\sqrt{1 + 8q} - 1}{2}\right). \tag{21}$$

Note that θ_1 is not defined for $q < 1/2$. For $q > 1/2$, $\theta_1 > \theta_2$.

Note that $\det A$ is *discontinuous* for (x_1^c, x_2^c) on the ellipse $(x_1^c/R)^2 + (x_2^c/R\cos\theta)^2 = 1$ [see Eqs.(14)], i.e., on the edge of the disk, just as in the face-on disk case. If $\det A(x \to 0) = +\infty$, $\det A$ changes sign at (x_1^c, x_2^c), which describes effectively a "critical curve", and the corresponding source positions give us a "caustic".

First we consider $q < 1/2$. Here we always have $C_1 < 0$. We have two different cases: (1) $\theta < \theta_2$, $C_2 < 0$, $S < 0$, $\det A(x \to 0) = -\infty$, we have only one true critical curve and it encloses $x = 0$; (2) $\theta > \theta_2$, $C_2 > 0$, $S > 0$ [$\det A(x \to 0) = +\infty$] if $|x_2| > \sqrt{|C_1|/C_2}\,|x_1|$, $S < 0$ [$\det A(x \to 0) = -\infty$] if $|x_2| < \sqrt{|C_1|/C_2}\,|x_1|$, here we have one true critical curve enclosing $x = 0$, plus an additional "critical curve" which is hourglass shaped and passes through $x = 0$, and is closed off by (x_1^c, x_2^c) defined above. Figs.1-3 show the critical curves (a) and caustics (b) for $q = 0.2$ ($\theta_2 = 72.168°$), for $\theta = 70°$, $75°$, and $85°$ respectively. The unit radius circle in (a) indicates the critical curve for the SIS only case (its corresponding caustic shrinks to the point $y = 0$ in the source plane); the unit radius circle in (b) indicates the multiple-image cross-section for the SIS only case.

For $q > 1/2$, we have three different cases: (1) $\theta < \theta_2$, $C_1 < 0$, $C_2 < 0$, $S < 0$, $\det A(x \to 0) = -\infty$, we have only one true critical curve and it encloses $x = 0$; (2) $\theta_2 < \theta < \theta_1$, $C_1 < 0$, $C_2 > 0$, $S > 0$ [$\det A(x \to 0) = +\infty$] if $|x_2| > \sqrt{|C_1|/C_2}\,|x_1|$, $S < 0$ [$\det A(x \to 0) = -\infty$] if $|x_2| < \sqrt{|C_1|/C_2}\,|x_1|$, here we have one true critical curve enclosing $x = 0$, plus an additional "critical curve" which is hourglass shaped and passes through $x = 0$, and is closed off by (x_1^c, x_2^c) defined above; (3) $\theta > \theta_1$, $C_1 > 0$, $C_2 > 0$, $S > 0$, $\det A(x \to 0) = +\infty$, we have two critical curves enclosing $x = 0$, one of them is the true critical curve, the other is given by (x_1^c, x_2^c) defined above. Figs.4-6 show the critical curves (a) and caustics (b) for $q = 0.6$ ($\theta_1 = 78.463°$, $\theta_2 = 45.238°$), for $\theta = 45°$, $75°$, and $85°$ respectively. The unit radius circles in the figures are the same as already indicated.

Because $\det A(\mathbf{x})$ is modified from Eq.(18) as we move away from $x = 0$, the hourglass shaped "critical curves" are given by the intersection of $|x_2| \sim \sqrt{|C_1|/C_2}\,|x_1|$ and the ellipse $(x_1^c/R)^2 + (x_2^c/R\cos\theta)^2 = 1$; this explains the curved sides of the hourglass shape. Due to numerical noise, some discrete points from the (x_1^c, x_2^c) ellipse and their corresponding source positions appear in Figs.1-6 as discrete points apart from the critical curves and caustics.

It is interesting to note that our study of the face-on disk case (see the previous section) suggests that the critical angle for the disk to contribute to image multiplicity is given by $\kappa^{disk} = q/\cos\theta = 1$, i.e., $\theta = \theta_0 \equiv \arccos(q)$. For $q < 1/2$, only θ_2 is defined, and $\theta_0 > \theta_2$; for $q > 1/2$, $\theta_1 > \theta_0 > \theta_2$. This indicates that an inclined disk is more efficient than a face-on

disk with the same surface mass density.

5. Increased multiple-image cross section due to the inclined disk

When there is only *one* critical curve (the true critical curve) in the **x** plane, the multiple image cross-section is given by the area enclosed by $y = 1$ plus the areas enclosed by the caustic which lies *outside* the $y = 1$ circle, which are two small sharp-angular areas lying along the y_1 axis; the caustic is completely inside the $y = 1$ circle for sufficiently small θ. When we have *two* branches of critical curves (one of them is a true critical curve, the other corresponds to discontinuity and change of sign in $\det A$) in the **x** plane, the multiple image cross-section is given by the area enclosed by $y = 1$ plus the areas enclosed by the caustics which lie *outside* the $y = 1$ circle, which now consist of two angular areas lying along the y_1 axis (corresponding to the true critical curve, at largest possible x), plus two round areas lying along the y_2 axis (corresponding to the "critical curve" due to discontinuity and change of sign in $\det A$).

Assuming uniform distribution of the inclination angle θ in solid angle, the average multiple-image cross section is

$$\overline{\sigma}_\theta = \frac{\int d\theta \, \sin\theta \, \sigma(\theta)}{\int d\theta \, \sin\theta}, \tag{22}$$

where $\sigma(\theta)$ is multiple-image cross section for inclination angle θ.

Figs.7-9 show the ratio of the multiple-image cross-sections for SIS plus inclined uniform disk and for SIS only, $\sigma(\theta)/\sigma^{SIS}$, as a function of the inclination angle θ, for three

groups (nine sets) of choices of (q, R). Table 1 lists the parameters and the corresponding average enhancement factor in multiple-image cross section $\overline{\sigma}_\theta / \sigma^{SIS}$.

Table 1: Average enhancement factor in multiple-image cross section

	$R = 1.5$	$R = 3$	$R = 6$
q=0.2	1.086	1.160	2.041
q=0.4	1.296	1.547	2.742
q=0.6	1.718	2.493	4.509

Let us write

$$q\,R = \frac{1.9}{\pi} \left(\frac{10\,\mathrm{kpc}}{r_{disk}} \right) \left(\frac{M_{disk}}{10^{11} M_\odot} \right) \left(\frac{150\,\mathrm{km/s}}{v_{SIS}} \right)^2. \tag{23}$$

For a model spiral galaxy with given $(v_{SIS}, M_{disk}, r_{disk})$, $q\,R$ is constant. Inspection of Table 1 shows that the modification of the galaxy's inclination averaged cross section is quite small, less than say 50% (there are other uncertainties in lens statistics calculations *at least* this large), if $q\,R$ is less than about unity. From equation (23) we then see that significant modification of the multiple image lensing cross section will only occur for objects with uncharacteristically small and massive disks and/or those with minimal spherical (halo) components. Few, if any, real galaxies may satisfy such conditions.

The differential probability of a strong-lensing (multiple-images) event is (Turner et al. 1984)

$$d\tau = n_L(z_d)\,\overline{\sigma}_\theta(z_d | z_s)\, \frac{c\,dt}{dz_d}\, dz_d, \tag{24}$$

where $n_L(z_d)$ is the number density of lenses at lens redshift z_d, $\overline{\sigma}_\theta(z_d|z_s)$ is the inclination-angle averaged cross-section for multiple images given source redshift z_s. From the above discussion, we would expect the total contribution of spiral galaxies to the QSO strong lensing optical depths to increase only slightly due to the effects of their thin disks. The optical depths would then continue to be dominated by early type galaxies.

However, the inclusion of an inclined disk breaks the circular symmetry due to the SIS, the true critical curve [where $\det A(x) = 0$] no longer maps to a point $(y = 0)$ as in the SIS only case, but maps to a caustic which encloses an area comparable to the SIS only multiple-image cross-section for $\theta > \theta_2$ [see Eq.(21)]. Since the magnification is infinite (for a point source) on the caustic, and decreases smoothly away from it, the cross section for high magnifications is significantly increased due to the inclusion of a disk. Quantitative investigation of this effect will require extensive numerical calculations which are outside the scope of this paper, but this effect may well be important. Observational selection effects favoring inclusion of high amplification (magnification) lensing configurations in flux limited samples can lead to major distortions of intrinsic distributions in real samples; see Ostriker & Vietri (1990), for example.

6.   Discussion and conclusion

We have examined strong (multiple image) gravitational lensing by spiral galaxies, modeled as infinitely thin uniform disks embedded in singular isothermal spheres. We

have derived general properties of the critical curves and caustics analytically. The multiple-image cross section is a sensitive function of the inclination angle of the disk relative to the observer. We have therefore computed the inclination averaged cross section for several sets of lensing parameters.

We find that the optical depth for multiply imaged QSOs should only increase by a factor of a few at most and by less than 50% in nearly all realistic cases; the inclusion of a disk is therefore expected to have *no* significant effect on the contribution of spiral galaxies to the total optical depth for multiply imaged QSOs. On the other hand, the cross section for high magnifications is significantly increased due to the inclusion of a disk. The increase in the number of lensed QSOs with high magnifications could have substantial effects on observed lens samples.

While completing this work, we became aware of recent preprints by Loeb (1997) and by Maller, Flores, and Primack (1997). The former is primarily concerned with the possible connectin between lensing by spiral galaxies and high column density HI absorption systems seen in QSO spectra but also briefly mentions the potential role of disk inclination in spiral galaxy lensing statistics. The subject of our paper overlaps partially with that of Maller *et al.*, and some of our results are qualitatively similar; however, our paper is mainly analytical (which provides insight into the mathematics of the critical curves and caustics) while theirs is numerical.

REFERENCES

Blandford, R. D. and Kochanek, C. S. 1987, ApJ, 321, 658.

Blandford, R. D. and Narayan, R. 1992, Ann. Rev. Astron. Astrophys., 30, 311.

Fukugita, M. and Turner, E. L. 1991, MNRAS, 253, 99.

Gott, J. R. and Gunn, J. E. 1974, ApJ Lett, 190, L105.

Keeton, C. R., Kochanek, C. S. and Seljak, U. 1996, CfA Preprint No. 4419.

Kochanek, C. S. and Blandford, R. D. 1987, ApJ, 321, 676.

Kochanek, C. S. 1991, ApJ, 379, 517.

Kochanek, C. S. 1993, ApJ, 419, 12.

Lawrence, C. R., Elston, R., Jannuzi, B. T. and Turner, E. L. 1995, Astron. J., 110, 2570.

Loeb, A. 1997, astro-ph/9701100.

Malhotra, S., Rhoads, J. E. and Turner, E. L. 1997, MNRAS, in press.

Maller, A.H., Flores, R.A., & Primack, J.R. 1997, astro-ph/9701110.

Maoz, D. and Rix, H.-W. 1993, ApJ, 416, 425.

Ostriker, J. P. and Peebles, P. J. E. 1973, ApJ, 183, 467.

Ostriker, J. P. and Vietri, M. 1990, Nature, 344, 45.

Schneider, P., Ehlers, J., & Falco, E.E., (ed. Springer-Verlag, Berlin, 1992), "Gravitational lenses".

Turner, E. L. 1980, ApJ Lett, 242, L135.

Turner, E. L., Ostriker, J. P., & Gott, J. R. (1984), ApJ, 284, 1.
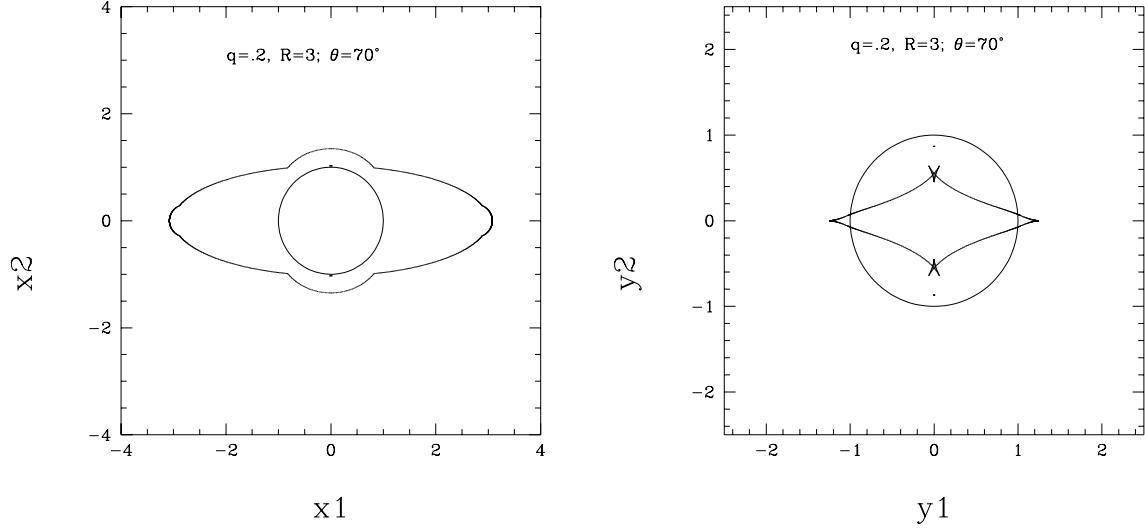
Fig. 1.— $q = 0.2$, $R = 3$, $\theta = 70° < \theta_2 = 72.168°$. (a) Critical curve. The unit radius circle indicates the critical curve for the SIS only case (its maps to $y = 0$ in the source plane). (b) Caustic. The unit radius circle indicates the multiple-image cross-section for the SIS only case.
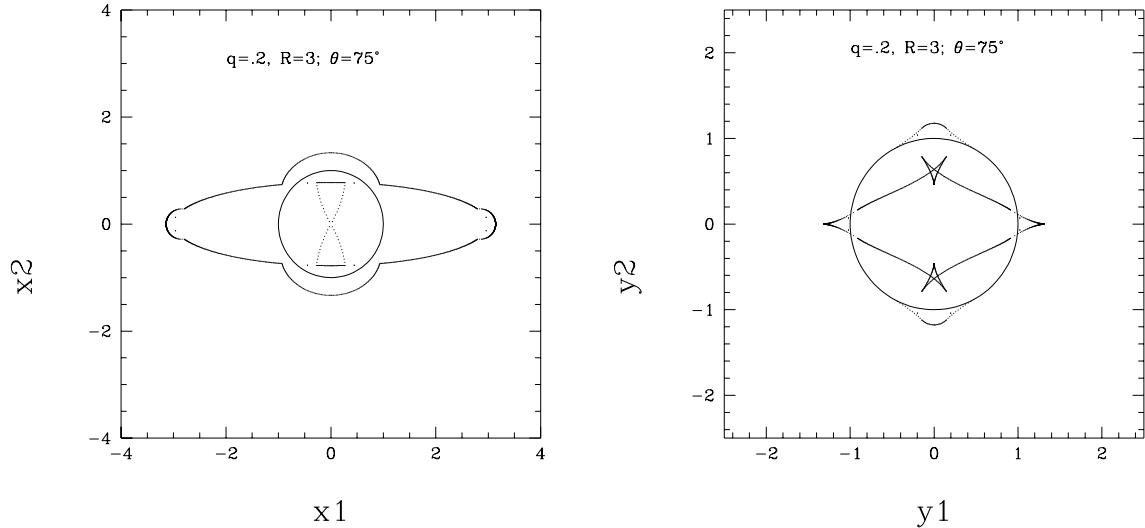
Fig. 2.— $q = 0.2$, $R = 3$, $\theta = 75° > \theta_2 = 72.168°$. The unit radius circles are the same as in

Fig.1. (a) Critical curve. (b) Caustic.
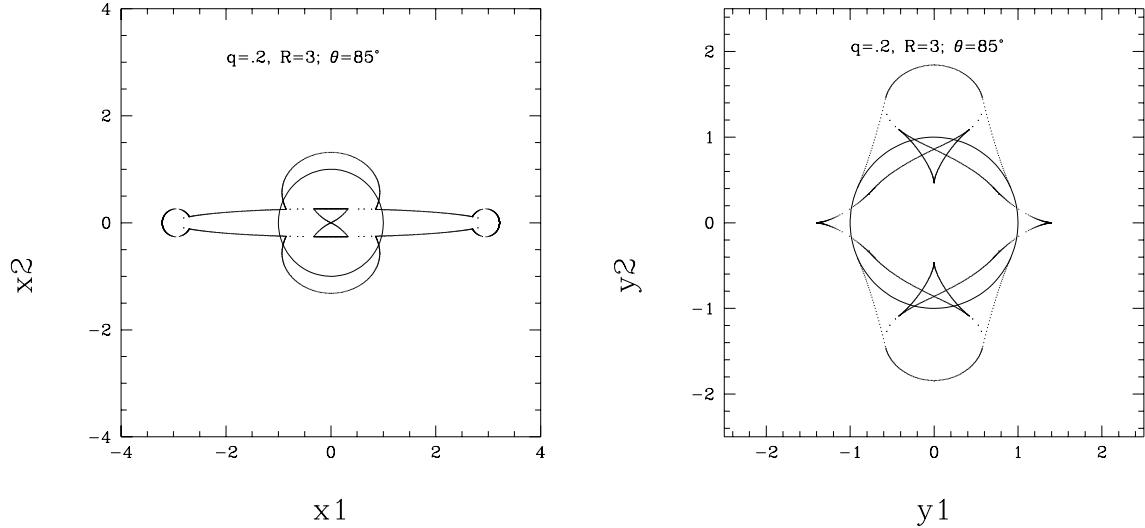

Fig. 3.— $q = 0.2$, $R = 3$, $\theta = 85° > \theta_2 = 72.168°$. The unit radius circles are the same as in

Fig.1. (a) Critical curve. (b) Caustic.
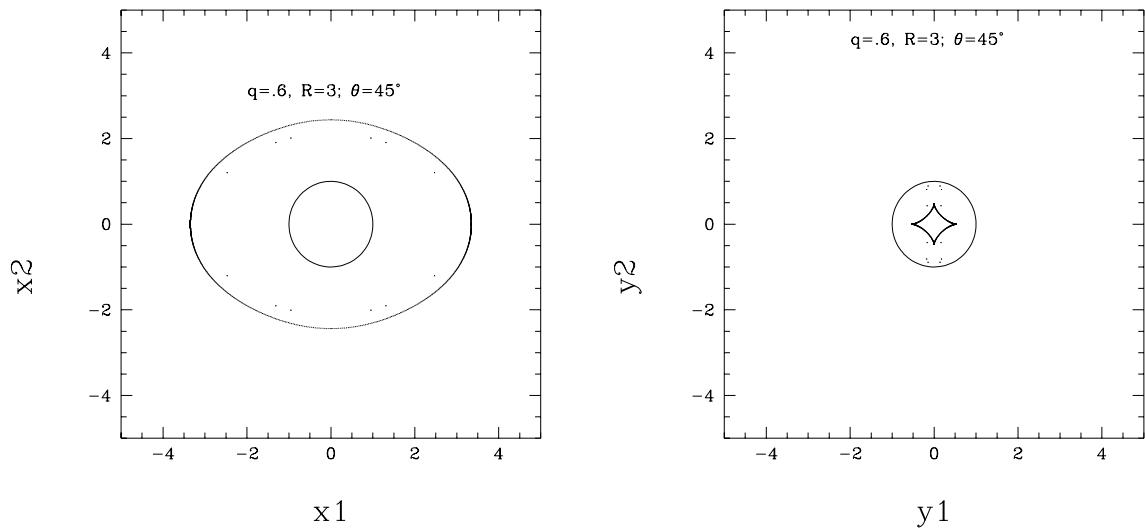
Fig. 4.— $q = 0.6$, $R = 3$, $\theta = 45° < \theta_2 = 45.238°$. The unit radius circles are the same as in

Fig.1. (a) Critical curve. (b) Caustic.
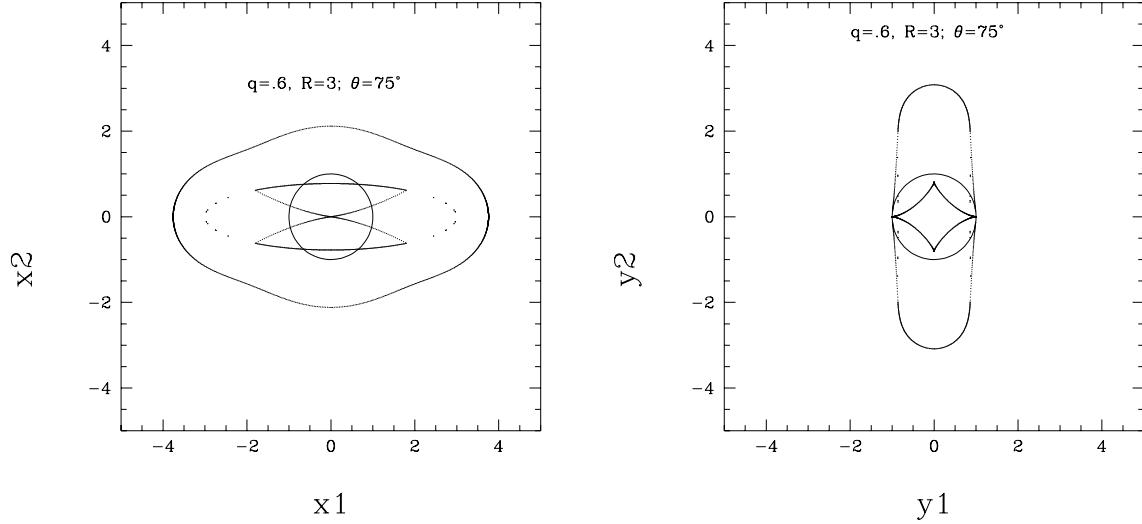
Fig. 5.— $q = 0.6$, $R = 3$, $\theta_2 = 45.238° < \theta = 75° < \theta_1 = 78.463°$. The unit radius circles are the same as in Fig.1. (a) Critical curve. (b) Caustic.
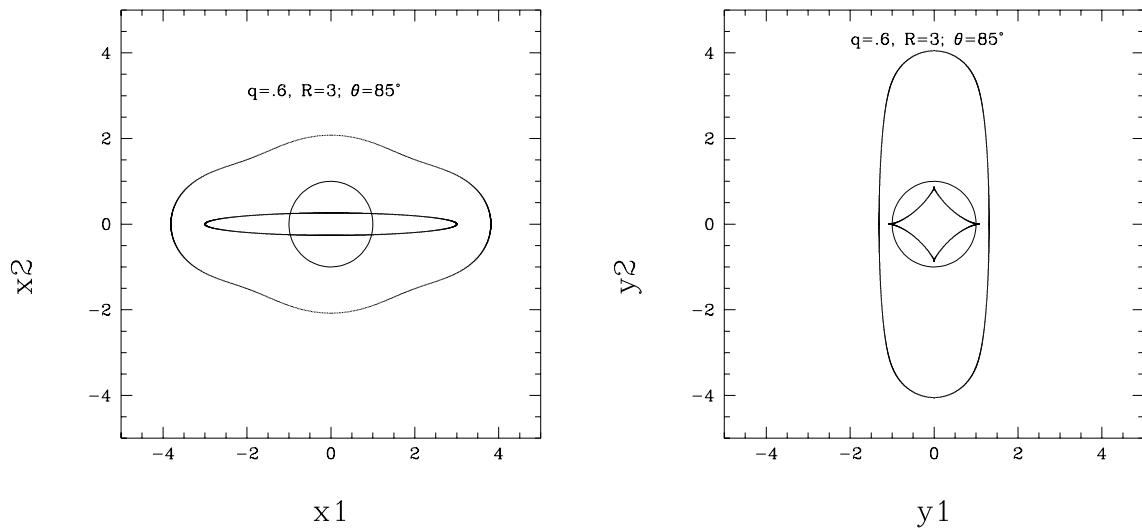
Fig. 6.— $q = 0.6$, $R = 3$, $\theta = 85° > \theta_1 = 78.463°$. The unit radius circles are the same as in Fig.1. (a) Critical curve. (b) Caustic.
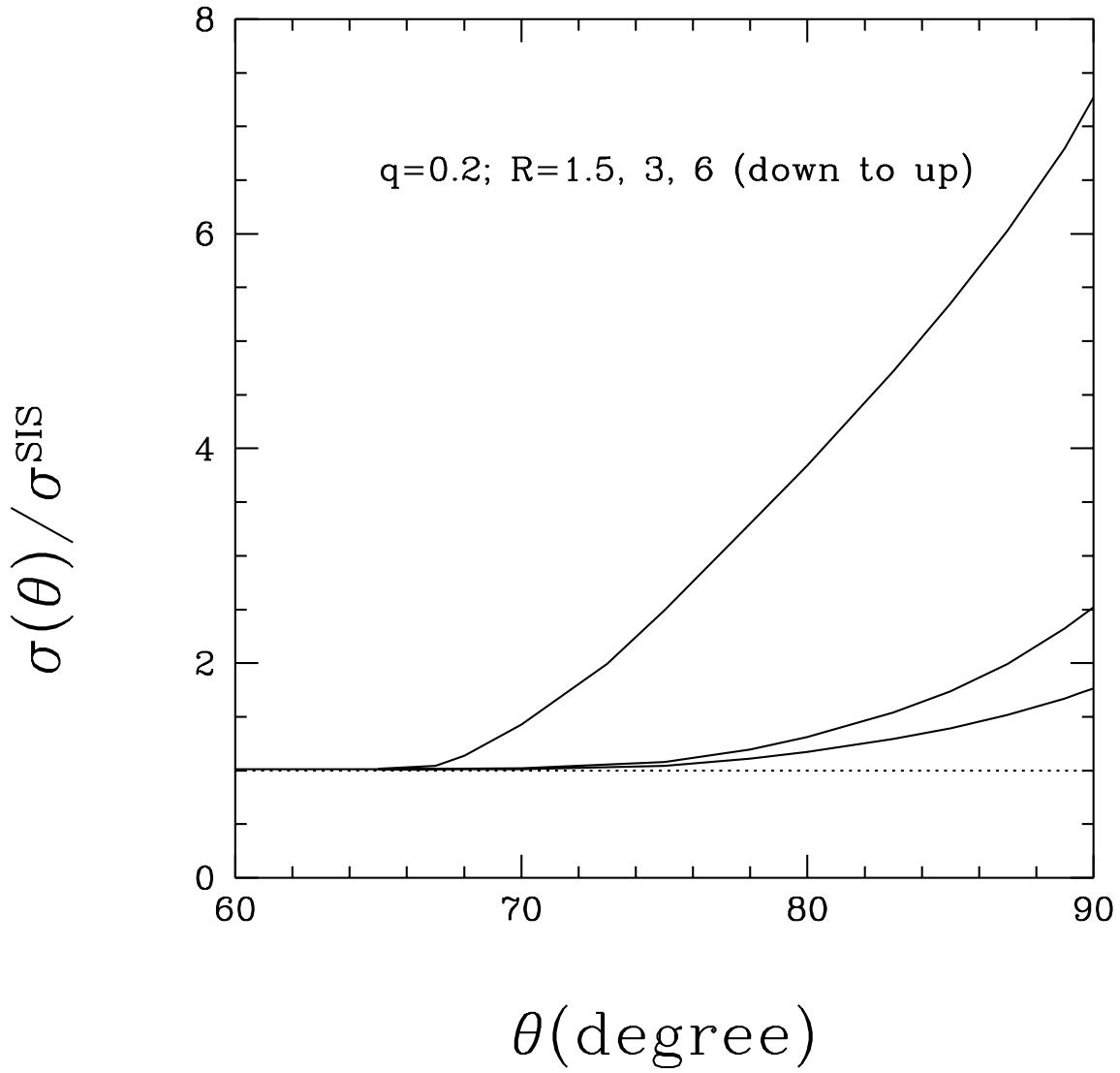
Fig. 7.— The ratio of the multiple-image cross-sections for SIS plus inclined uniform disk and for SIS only, $\sigma(\theta)/\sigma^{SIS}$, as a function of the inclination angle θ, for $q = 0.2$, $R = 1.5$, 3, 6.
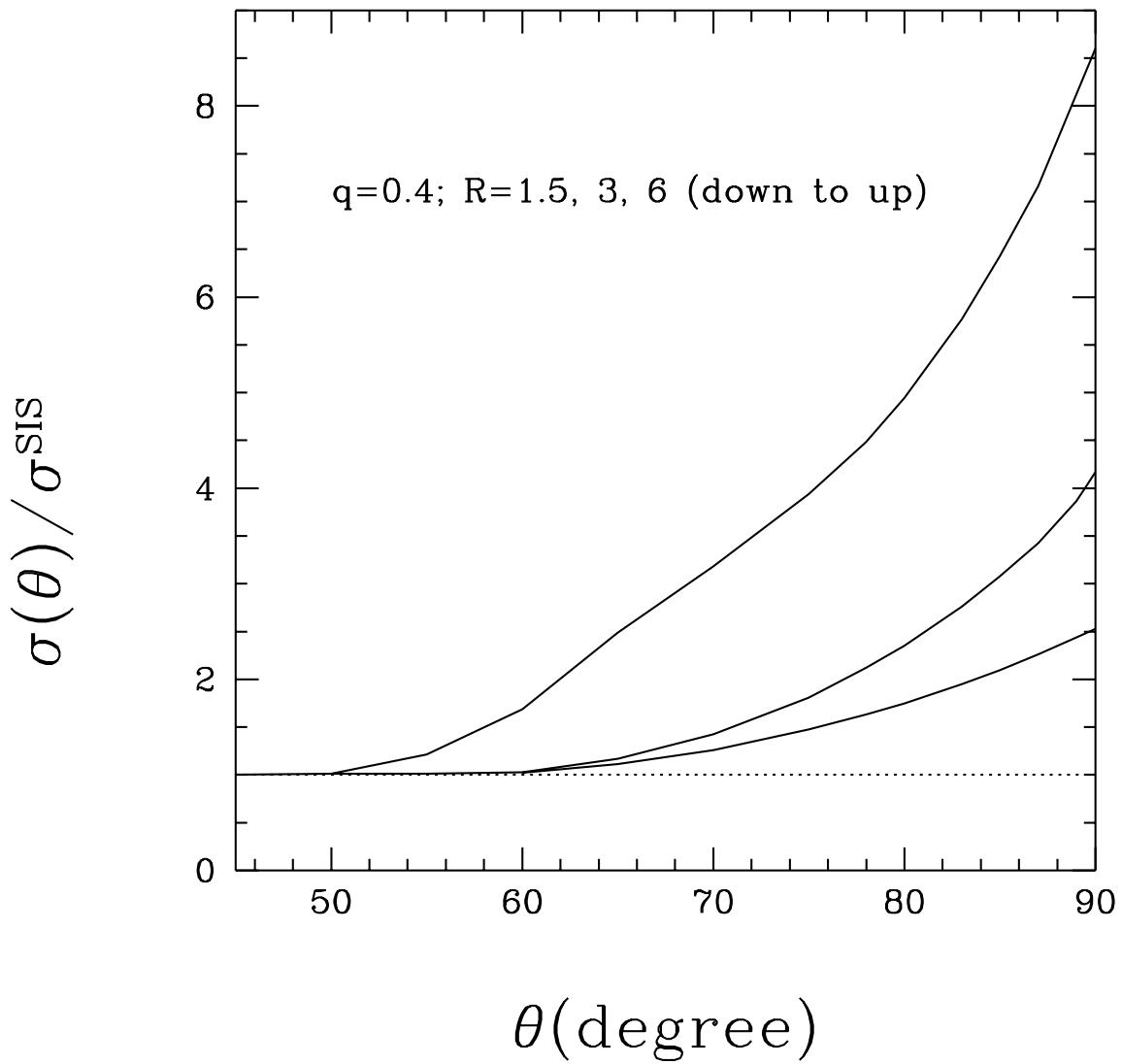
Fig. 8.— Same as Fig.7, for $q = 0.4$, $R = 1.5, 3, 6$.
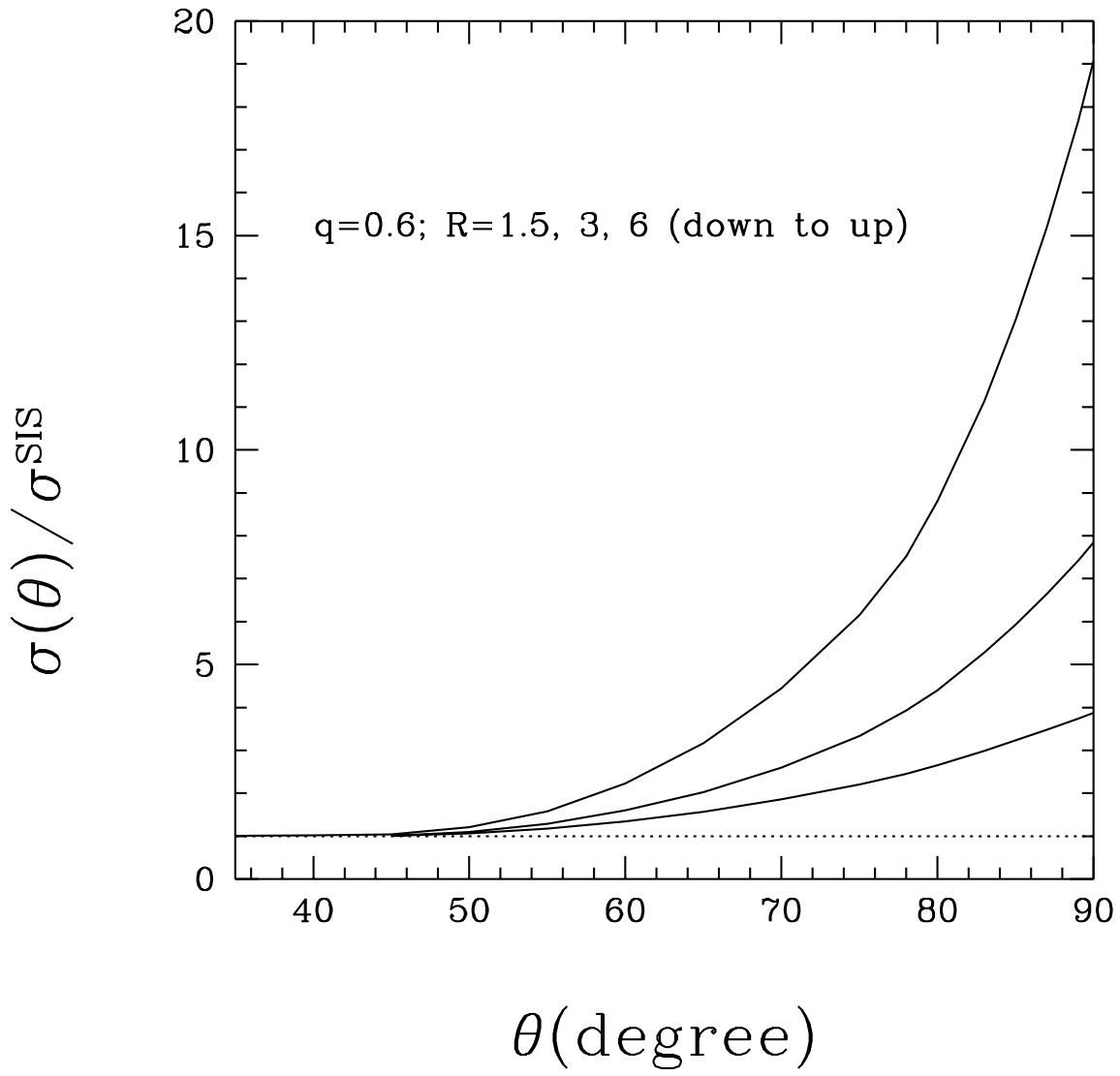
Fig. 9.— Same as Fig.7, for $q = 0.6$, $R = 1.5$, 3, 6.